Experimental investigation of the stability of Fe-rich carbonates in the lower mantle

E. Boulard, N. Menguy, Anne-Line Auzende, K. Benzerara, H. Bureau, D. Antonangeli, A. Corgne, Guillaume Morard, J. Siebert, Jean-Philippe Perrillat, et al.

Experimental investigation of the stability of Fe-rich carbonates in the lower mantle

E. Boulard,[1,2] N. Menguy,[1] A. L. Auzende,[1] K. Benzerara,[1] H. Bureau,[1] D. Antonangeli,[1] A. Corgne,[1,3] G. Morard,[1] J. Siebert,[1] J. P. Perrillat,[4,5] F. Guyot,[1] and G. Fiquet[1]

Received 29 July 2011; revised 2 December 2011; accepted 13 December 2011; published 10 February 2012.

[1] The fate of carbonates in the Earth's mantle plays a key role in the geodynamical carbon cycle. Although iron is a major component of the Earth's lower mantle, the stability of Fe-bearing carbonates has rarely been studied. Here we present experimental results on the stability of Fe-rich carbonates at pressures ranging from 40 to 105 GPa and temperatures of 1450–3600 K, corresponding to depths within the Earth's lower mantle of about 1000–2400 km. Samples of iron oxides and iron-magnesium oxides were loaded into CO_2 gas and laser heated in a diamond-anvil cell. The nature of crystalline run products was determined in situ by X-ray diffraction, and the recovered samples were studied by analytical transmission electron microscopy and scanning transmission X-ray microscopy. We show that $Fe^{(II)}$ is systematically involved in redox reactions with CO_2 yielding to $Fe^{(III)}$-bearing phases and diamonds. We also report a new $Fe^{(III)}$-bearing high-pressure phase resulting from the transformation of $FeCO_3$ at pressures exceeding 40 GPa. The presence of both diamonds and an oxidized C-bearing phase suggests that oxidized and reduced forms of carbon might coexist in the deep mantle. Finally, the observed reactions potentially provide a new mechanism for diamond formation at great depth.

Citation: Boulard, E., et al. (2012), Experimental investigation of the stability of Fe-rich carbonates in the lower mantle, *J. Geophys. Res.*, *117*, B02208, doi:10.1029/2011JB008733.

1. Introduction

[2] Carbon exchange between the Earth's interior and the surface occurs over time scales of billions of years and constitutes the geodynamical carbon cycle. Carbon (C) is recycled by means of subduction into the deep Earth, mainly as carbonates. Little is known about the extent of the deep mantle cycle that largely depends on the preservation of carbonates during subduction processes. Previous experimental studies discussed the possibility of having the transport of carbon down to the transition zone and lower mantle [e.g., *Yaxley and Green*, 1994; *Molina and Poli*, 2000; *Poli and Schmidt*, 2002; *Seto et al.*, 2008]. Carbonates from sedimentary material and altered basalts [e.g., *Alt and Teagle*, 1999] preserved during subduction are estimated to account for a flux of 3.6×10^{12} mol/year of carbon being returned into the deep mantle [*Sleep and Zahnle*, 2001; *Macpherson et al.*, 2010]. This quantity would represent about 10 to 30 wt % of the carbon reservoir in the primitive mantle [*Javoy*, 1997; *Lécuyer et al.*, 2000]. Because of its very low solubility in deep Earth's minerals [e.g., *Keppler et al.*, 2003; *Shcheka et al.*, 2006], carbon is expected to be present as accessory phases in the mantle, either as (1) oxidized phases such as carbonates [e.g., *Isshiki et al.*, 2004] and carbonated fluids or melt [e.g., *Canil*, 1990] or (2) reduced phases such as diamonds or Fe-C alloys (see *Dasgupta and Hirschmann* [2010] for a review). The carbon redox state and the nature of the carbon-bearing phases under lower mantle conditions are still unknown. It is commonly considered that the lower mantle may be too reduced to host carbonates [*McCammon*, 2006; *Frost and McCammon*, 2008; *Rohrbach and Schmidt*, 2011]. However, locally carbonate-enriched areas, such as subducting slabs, might contribute to preserve oxidized carbon-bearing phases in the deep mantle [*Litasov and Ohtani*, 2010]. Moreover, diamonds formed in the lower mantle have been reported to occasionally contain carbonate inclusions, suggesting the presence of carbonates in the deep Earth and a possible coexistence of reduced and oxidized species [*Stachel et al.*, 2000; *Brenker et al.*, 2007].

[3] At the Earth's surface, carbonates usually occur as three main phases: $CaCO_3$ (calcite), $CaMg(CO_3)_2$ (dolomite), and $MgCO_3$ (magnesite). Because of reactions between solid carbonates and silicates such as pyroxenes and silicate-perovskite [*Biellmann et al.*, 1993; *Wood et al.*, 1996], Mg-Fe carbonates should represent the dominant oxidized

[1]Institut de Minéralogie et de Physique des Milieux Condensés, Institut de Physique du Globe de Paris, Université Pierre et Marie Curie, UMR 7590, CNRS, Université Paris Diderot, Paris, France.
[2]Department of Geological and Environmental Sciences, Stanford University, Stanford, California, USA.
[3]Institut de Recherche en Astrophysique et Planétologie, UMR 5277, Université de Toulouse, CNRS, Toulouse, France.
[4]European Synchrotron Radiation Facility, Grenoble, France.
[5]Laboratoire de Géologie de Lyon, UMR 5276, Université Claude Bernard Lyon 1, CNRS, ENS Lyon, Villeurbanne, France.

0148-0227/12/2011JB008733

Table 1. Experimental Conditions, Run Products, and Analytical Methods Used[a]

Run	Starting Materials	P(GPa)	T(K)	Run Products	Analytical Method(s)
1	$FeO + CO_2$	40	1460	Carb. + h-Mt + D (+ $Fe_4(CO_4)_3$)	XRD
		50	2280	Carb. + h-Mt + D (+ $Fe_4(CO_4)_3$)	XRD, ATEM
2	$FeO + CO_2$	60	2380	Wus. + h-Mt + D + $Fe_4(CO_4)_3$ (+ Carb.)	XRD, ATEM
3	$FeO + CO_2$	75	2180	Wus. + h-Mt + D + $Fe_4(CO_4)_3$	XRD, ATEM, STXM
4	$FeO + CO_2$	70	2480	h-Mt + D+ $Fe_4(CO_4)_3$	XRD
		95	2640	h-Mt + D + $Fe_4(CO_4)_3$	XRD, ATEM, STXM
5	$FeO + CO_2$	97	2270	h-Mt + D + $Fe_4(CO_4)_3$	XRD
6	$FeO(OH) + CO_2$	55	2000	h-Mt. (+ D?) + $Fe_4(CO_4)_3$ + α-FeO(OH) + ε-FeO(OH)	XRD
7	$Fe_2O_3 + CO_2$	88	2500	$Fe_4(CO_4)_3$ + α -Fe_2O_3	XRD
8	$(Mg_{0.6}Fe_{0.4})O + CO_2$	55	2020	Fp + Carb. + h-Mt + D	XRD, ATEM, STXM
9	$(Mg_{0.6}Fe_{0.4})O + CO_2$	75	2670	Fp + h-Mt + HP-$(MgFe)CO_3$ + D	XRD
10	$(Mg_{0.6}Fe_{0.4})O + CO_2$	97	3650	Fp + h-Mt + HP-$(MgFe)CO_3$ + D	XRD, ATEM, STXM
11	$(Mg_{0.6}Fe_{0.4})O + CO_2$	105	2850	Fp + h-Mt + HP-$(MgFe)CO_3$ + D	XRD, ATEM, STXM

[a]Pressure and temperature uncertainties are ± 5 GPa and ± 150 K, respectively. Abbreviations are as follows: Carb., Carbonate; h-Mt, high-pressure magnetite phase; D, Diamond; Fp, Ferropericlase; Wus., Wüstite; α-FeO(OH), low-pressure polymorph of goethite; ε-FeO(OH), the high-pressure polymorph of goethite; α -Fe_2O_3, the high-pressure polymorph of hematite; $Fe_4(CO_4)_3$, high-pressure high-temperature phase obtained from $FeO + CO_2$ as described in this paper; HP-$(MgFe)CO_3$, high-pressure phase of $(Mg, Fe)CO_3$ described by *Boulard et al.* [2011]; XRD, X-ray diffraction; ATEM, analytical transmission electron microscopy; STXM, scanning transmission X-ray microscopy.

carbon-bearing phase in the lower mantle. This is supported by the great stability of magnesite at high pressures and high temperatures [e.g., *Katsura et al.*, 1991; *Biellmann et al.*, 1993; *Fiquet et al.*, 2002; *Isshiki et al.*, 2004]. However, some doubts have remained regarding the nature of C-bearing phases in the deep mantle because of the lack of experimental data on Fe-bearing carbonates.

[4] Recently, *Boulard et al.* [2011] experimentally confirmed the theoretical expectations [*Skorodumova et al.*, 2005; *Oganov et al.*, 2008; *Panero and Kabbes*, 2008] of a high-pressure polymorph of $MgCO_3$ at pressures above 80 GPa and temperatures above ~2300 K. This phase is characterized by a structure based on three-membered rings of corner-sharing $(CO_4)^{4-}$ tetrahedra, thus suggesting possible new silicate-like carbonate polymorphs. A similar structure was also observed in the case of Fe-bearing magnesite ($(Mg,Fe)CO_3$) [*Boulard et al.*, 2011]. In the latter, the formation of the new high-pressure phase was associated with oxidation of $Fe^{(II)}$ to $Fe^{(III)}$ and production of reduced carbon compounds such as diamonds or CO.

[5] The goal of the present study is to investigate the $(Mg,Fe)CO_3$ system on broader pressure and compositional ranges in order to gain additional insight into the behavior of Mg-Fe carbonates along relevant subduction *P-T* paths in the lower mantle. Here, we investigate the stability of carbonates at high pressures by studying the recombination of oxides into carbonates rather than the decomposition or transformation of carbonate starting materials. This "reversal" approach is expected to increase the chances of discovering thermodynamically stable phases rather than metastable intermediate states. For this purpose, samples were synthesized in a laser-heated diamond-anvil cell and characterized in situ by X-ray diffraction and ex situ by analytical transmission electron microscopy and scanning transmission X-ray microscopy. Special attention was dedicated to the behavior of the pure $FeO-CO_2$ end-member for which only few data exist. Additional experiments were conducted using $Fe^{(III)}$-bearing and hydrous phases as starting materials. As a whole, the experiments performed in this study allow us to discuss the nature of redox reactions in the $(Mg,Fe)CO_3$ system and hence to evaluate the stability of carbonate phases in subducting slabs.

2. Experimental and Analytical Techniques

2.1. High-Pressure and High-Temperature Experiments

[6] Experiments were conducted using symmetric Mao-Bell-type diamond-anvil cells (DAC) equipped with 200 μm flat or 300/150 μm beveled culet diamonds. In order to test the reactivity of oxides with CO_2, sintered powders of synthetic ferropericlase ($(Mg_{0.6},Fe_{0.4})O$), wüstite (FeO), hematite (Fe_2O_3), and a natural sample of goethite (FeO(OH)) from the Central African Republic, were loaded in CO_2. The CO_2 gas was loaded with a high-pressure gas-loading apparatus at room temperature and 600 bars. Oxides were thus isolated from diamonds by CO_2, preventing reactions with diamonds. For each run, pressure was directly increased to its target value and the sample was then heated up using the double-sided laser-heating system available on the high-pressure beamline ID-27 at the European Synchrotron Radiation Facility (ESRF). The samples were heated for ~2 h at 1500–3500 K to ensure a full transformation of the starting material. Pressure was measured using ruby fluorescence at room temperature [*Mao et al.*, 1986] and/or the equation of state of the observed phases such as ferropericlase [*Fei et al.*, 2007], the high-pressure polymorph of magnetite [*Haavik et al.*, 2000] and of goethite [*Gleason et al.*, 2008]. At high temperatures, thermal pressure corrections are of the order of +10%–15% of the initial pressure [*Fiquet et al.*, 2010]. Pressure uncertainties are estimated to be about ±5 GPa. Temperature was measured by spectroradiometric analysis of thermal radiation spectra [*Benedetti and Loubeyre*, 2004], with uncertainties of the order of ±150 K [*Morard et al.*, 2008]. A total of 11 runs were performed under pressures ranging between 40 and 105 GPa and temperatures between 1450 and 3600 K, corresponding to depths within the Earth of approximately 1000–2400 km. The experimental conditions and run products of each experiment are reported in Table 1.

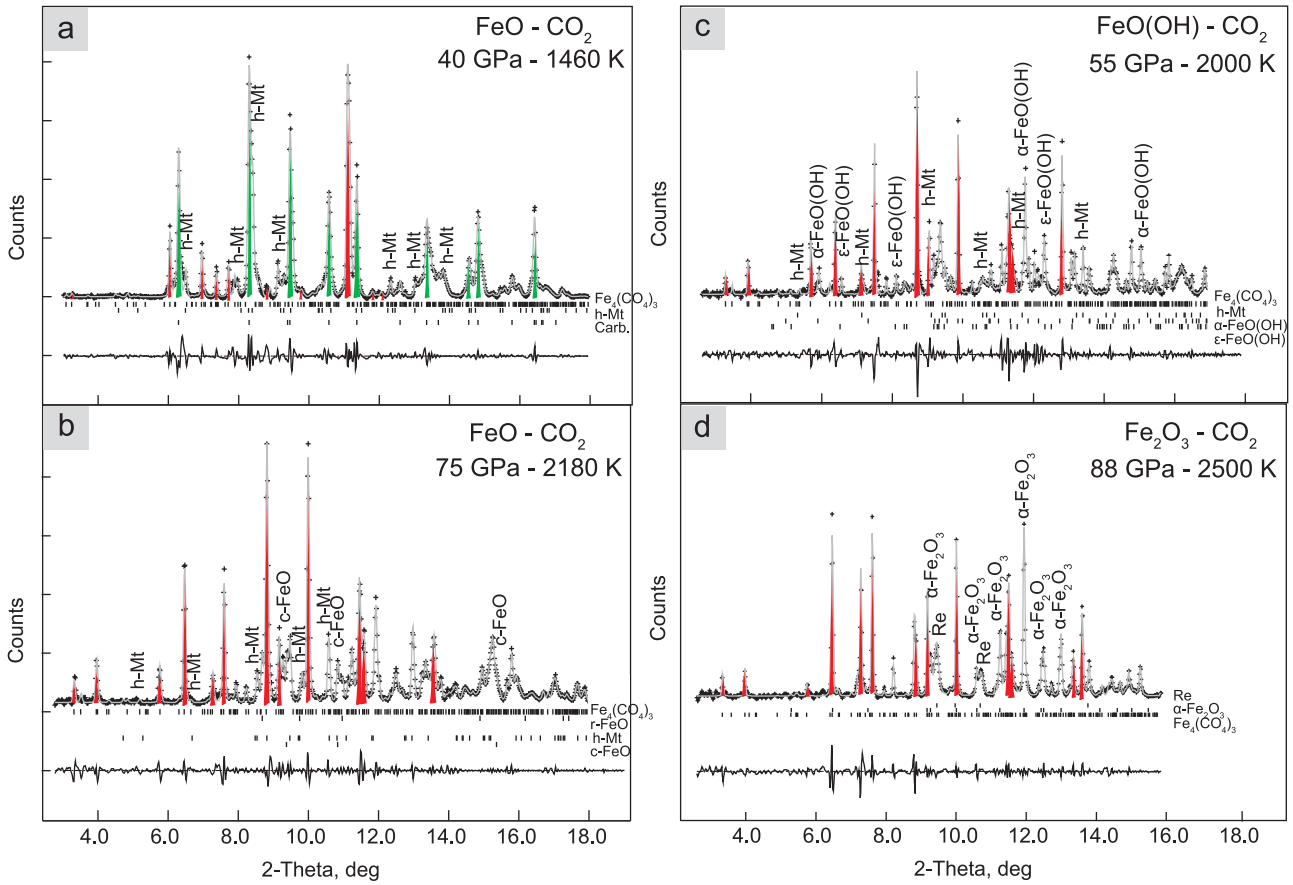

Figure 1. In situ X-ray diffraction patterns for $FeO/Fe_2O_3/FeO(OH)$ starting materials loaded in CO_2. Crosses represent observed data (background subtracted), and the solid lines show the profile refinements (λ = 0.3738 Å). Residuals between experiment and fit are shown below the diffraction pattern. Peaks assigned to siderite are in green, and main peaks assigned to the new Fe-C-O high-pressure phase are in red. Abbreviations on peaks are as follows: h-Mt, high-pressure magnetite [*Haavik et al.*, 2000]; α-Fe_2O_3, high-pressure hematite [*Ono et al.*, 2004]; c-FeO, FeO in B1 structure; r-FeO, rombohedral FeO [*Yagi et al.*, 1985]; α-FeO(OH), goethite; ε-FeO(OH), high-pressure polymorph of goethite [*Gleason et al.*, 2008]; Re, rhenium gasket; Carb., carbonate; $Fe_4(CO_4)_3$, high-pressure high-temperature form of siderite. Experimental conditions are written in each diagram.

2.2. X-Ray Diffraction

[7] Angle-dispersive X-ray diffraction spectra were collected in situ at high pressures and high temperatures. The details of the experimental setup are reported elsewhere [*Mezouar et al.*, 2005]. The incident X-ray beam was monochromatized to a wavelength of 0.3738 Å. Typical exposure time was 90 s at high pressures and high temperatures. The diffraction images were integrated with the Fit2d software [*Hammersley et al.*, 1996]. The one-dimensional diffraction patterns were treated with the General Structure Analysis System (GSAS) software package [*Larson and Von Dreele*, 1994] using the LeBail method to identify the different phases and refine lattice parameters.

2.3. Focused Ion Beam (FIB) Milling

[8] This technique was employed to prepare the recovered samples for analyses by transmission electron microscopy (TEM), scanning transmission electron microscopy (STEM), and scanning transmission X-ray microscopy (STXM). Focused ion beam (FIB) thin sections were extracted from the center of laser-heated spots and thinned to electron transparency (~100 nm thickness) with a focused Ga^+ ion beam operating at 30 kV and currents from 20 nA down to 1 pA for final surfacing. FIB milling was performed with a FEI STRATA DB 235 at IEMN (Lille, France), a Philips FIB 200 transmission electron microscope (TEM) at CP2M (Marseille, France), and a Zeiss Crossbeam Neon40 at Institut de Minéralogie et de Physique des Milieux Condensés (IMPMC) (Paris, France). A detailed description of the FIB sample preparation technique for high-pressure samples can be found in the works by *Auzende et al.* [2008] and *Fiquet et al.* [2010].

2.4. Scanning Transmission X-Ray Microscopy (STXM)

[9] STXM provides both imaging and high-spatial high-energy resolution X-ray absorption spectra. This gives information on element speciation and local environment. Near- edge X-ray absorption fine structure spectroscopy (NEXAFS) data were obtained by performing image stacks,

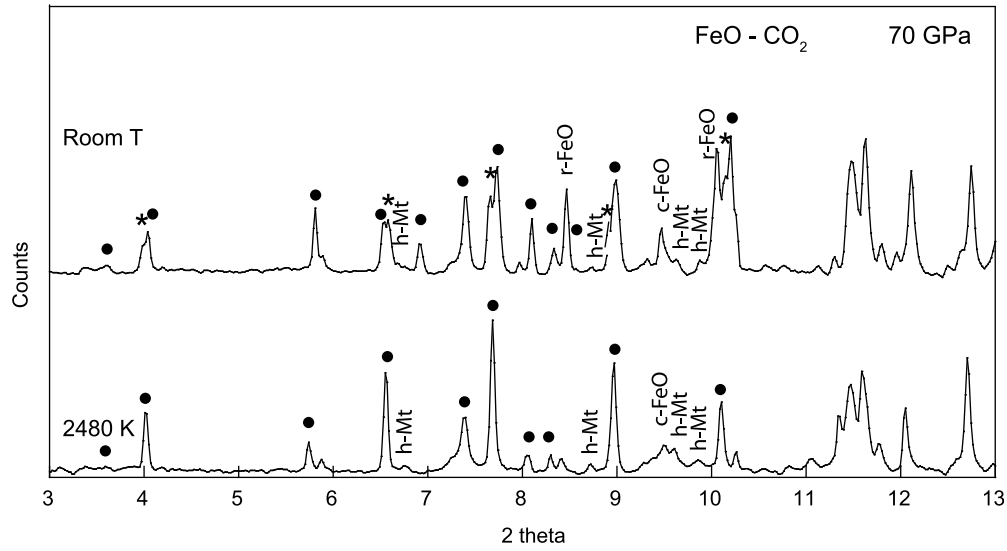

Figure 2. X-ray diffraction patterns from run 4 ($FeO + CO_2$ transformed at 70 GPa and 2480 K) in situ at high pressures and high temperatures and after temperature quenching ($\lambda = 0.3738$ Å). New peaks marked by stars reveal a transformation into a different phase on temperature quenching of the high-pressure high-temperature form of siderite (black circles). Abbreviations on peaks are as follows: h-Mt, high-pressure magnetite [*Haavik et al.*, 2000]; c-FeO, FeO in B1 structure; r-FeO, rombohedral FeO [*Yagi et al.*, 1985].

which were collected by scanning the sample with energy increments of 0.1 eV over the energy range of interest (280 to 310 eV for the carbon K edge, 700 to 730 eV for iron $L_{2,3}$ edges). The stack image procedure thus consists of measuring the NEXAFS spectrum of a specific element at each pixel (one pixel can be as small as 30 nm) of the image. Counting times were a few milliseconds or less per pixel. Part of the STXM work was performed at the Advanced Light Source (ALS) (Lawrence Berkeley National Laboratory) on branch line 11.0.2.2 and the other part at the spectromicroscopy beamline 10ID-1 at the Canadian Light Source (CLS, Saskatoon, Canada). The ALS storage ring operated at 1.9 GeV and 200–500 mA stored current. A 1200 l/mm grating and 25 μm exit slits in both dispersive and non-dispersive modes were used for carbon imaging and spectroscopy, providing a theoretical energy resolution better than 50 meV. A 1200 l/mm grating and 10 μm exit slit were used for mapping at the Fe $L_{2,3}$ edges. The energy scales for this study were calibrated using the well-resolved 3*p* Rydberg peak of gaseous CO_2 for the C K edge [*Ma et al.*, 1991] and the major peak of hematite at 708.7 eV for the Fe $L_{2,3}$ edges. Normalization and background corrections of the Fe $L_{2,3}$ edges and C K edge NEXAFS spectra were performed by dividing each spectrum by a second spectrum from a Fe- or C-free location in the same sample. Rationale for STXM data acquisition and analysis at the C K edge and Fe $L_{2,3}$ edges can be found in the works by *Benzerara et al.* [2004] and *Miot et al.* [2009].

2.5. Transmission Electron Microscopy

[10] Complementary to STXM, analytical transmission electron microscopy (ATEM) was carried out on the FIB thin sections in order to help with phase identification and to obtain chemical analyses on individual phases. ATEM was performed at IMPMC (Paris, France) with a JEOL 2100-F operating at 200 keV, equipped with a field emission gun. Samples were observed in TEM and STEM modes for which a high-angle annular darkfield (HAADF) detector was used. Semiquantitative information on the sample chemistry was obtained by X-ray energy dispersive spectrometry (XEDS), and selected area electron diffraction (SAED) patterns were used for phase identification. Electron energy loss spectroscopy (EELS) was performed in the TEM mode using a dispersion of 0.3 eV per channel to record spectra in the ranges of 480–800 eV (O K and Fe $L_{2,3}$ edges) and 250–560 eV (O and C K edges). The final energy resolution measured as the width of the zero-loss peak (ZLP) at half height was 1.3 eV. An indicative stoichiometry of the product phases was obtained using the conventional Egerton method of extraction [*Egerton*, 1996] and Hatree-Slater cross-section calculation. This method provided elemental ratios such as Fe/C, Fe/O and C/O.

3. Results

3.1. FeO-Fe_2O_3-CO_2 System

[11] Five runs were conducted with wüstite (FeO) loaded in CO_2 at pressures between 40 and 97 GPa (runs 1–5 of Table 1). In each of these runs, a small contribution from the starting material remained in the diffraction patterns of the transformed samples. The high-pressure phase of CO_2 described by *Iota et al.* [1999] was not identified, possibly because of the low *Z* number of CO_2 compared with that of Fe-bearing phases. In the two runs at 40–50 and 60 GPa (runs 1 and 2), in situ X-ray diffraction (XRD) patterns collected at high pressures and high temperatures show the presence of $FeCO_3$ siderite, with space group *R*-3*c*, together with the high-pressure polymorph of magnetite [*Haavik et al.*, 2000] and a new phase (Figure 1a). This new phase is characterized by the presence of several new peaks

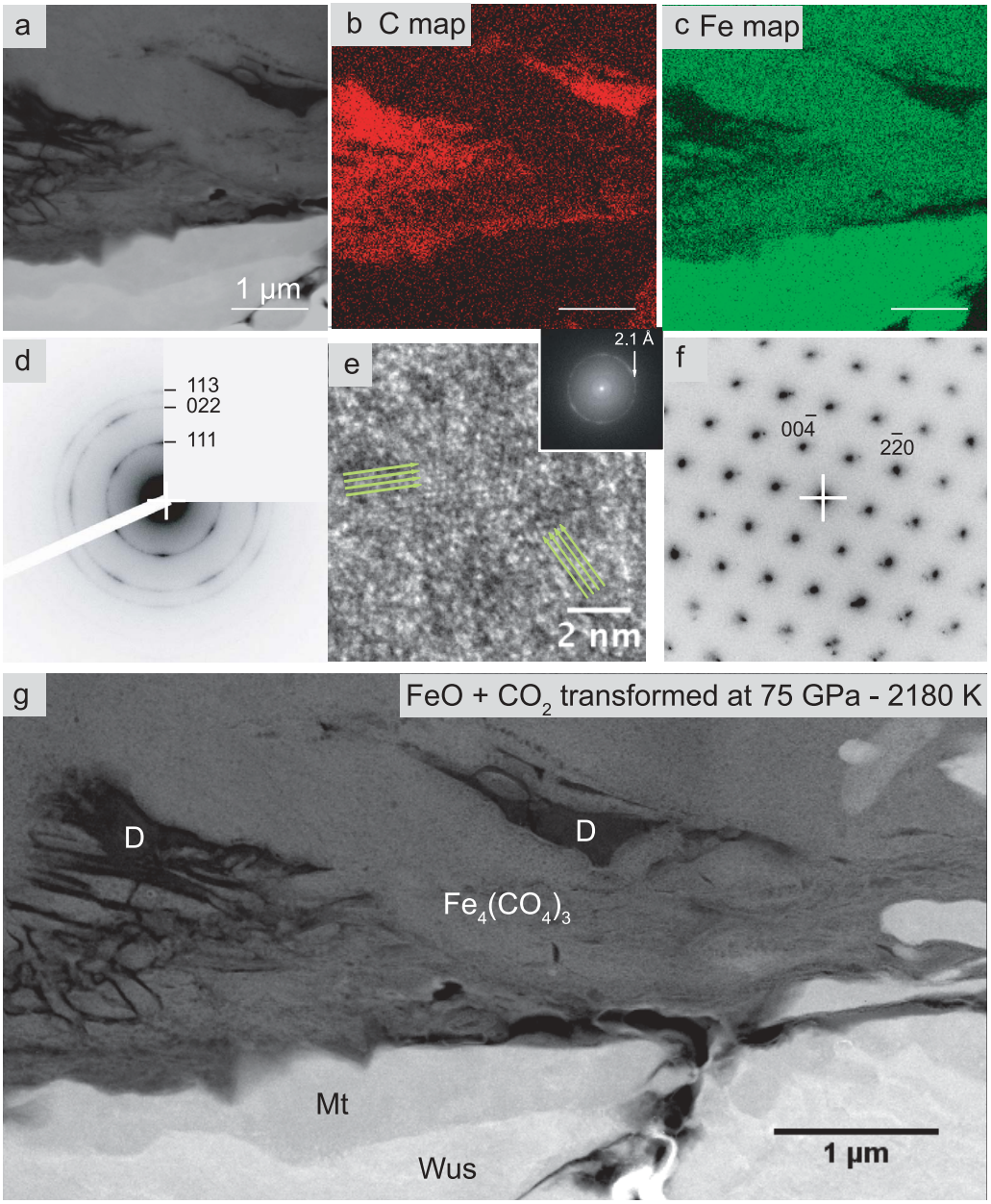

Figure 3. Analytical transmission electron microscopy of FeO starting material loaded in CO_2 recovered after transformation at 75 GPa and 2180 K (run 3). (a) STEM image of the area analyzed by XEDS, (b) carbon XEDS mapping, (c) iron XEDS mapping. The upper part of the FIB thin section is C and Fe rich. Nanodiamonds appear in light red in Figure 3b, and iron oxides (wüstite and magnetite) appear in light green in Figure 3c. (d) Electron diffraction of nanodiamonds. Distances at 2.08 ± 0.05, 1.27 ± 0.05, and 1.08 ± 0.05 Å are indexed as (111), (022), and (113) lattice planes of diamond respectively. (e) High-resolution TEM picture of nanodiamonds together with the Fourier transform diagram of the image area. Arrows highlight the periodicity 111 of ~2.1 Å intervals. (f) Electron diffraction of magnetite along a zone axis [110]. Distances at 2.94 ± 0.05, 4.81 ± 0.05, and 2.08 ± 0.05 Å are indexed as (2–20), (1-1-1), and (00–4) lattice planes of magnetite, respectively. (g) STEM image showing the presence of four different phases: wüstite (Wus), magnetite (Mt), nanodiamonds (D), and the new $Fe_4(CO_4)_3$ phase.

especially at high *d* spacings. At pressures above 60 GPa (runs 3, 4, and 5), the reflection lines of siderite disappeared and only this new high-pressure phase was observed (Figure 1b). The new phase undergoes a structural transformation, with the quenched structure being different from that of siderite on quenching to room temperature (Figure 2).

[12] Selected TEM results obtained on the recovered sample of run 3, after transformation of FeO + CO_2 at 75 GPa and 2180 K, are reported in Figure 3. Figure 3a displays a HAADF STEM picture of a portion of the FIB slice where XEDS analyses were carried out. The chemical map of carbon presented in Figure 3b reveals the existence

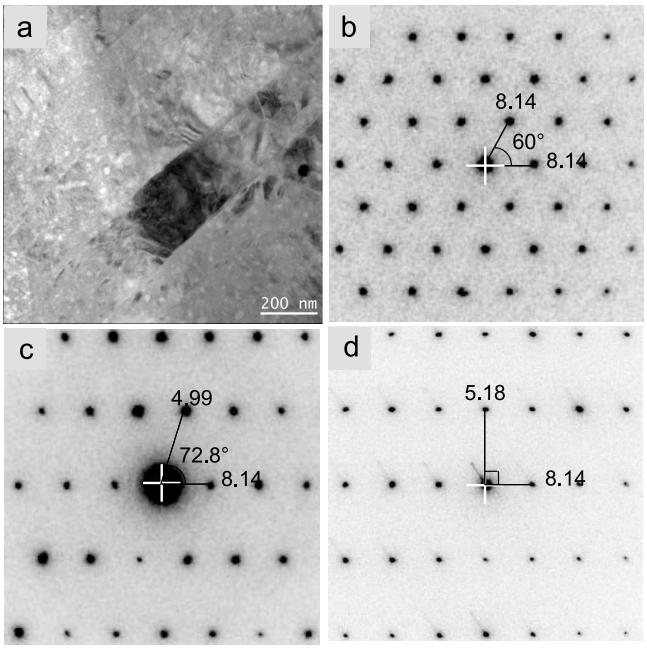

Figure 4. (a)TEM picture and (b–d) electron diffraction images of the new Fe-C-O-rich phase after back transformation at ambient conditions. Measured *d* spacings and angles are given.

of nanodiamond clusters. The presence of diamonds at the nanometer scale was further confirmed by SAED (Figure 3d) and by high-resolution TEM (Figure 3e). Typical sizes of these diamond nanocrystals are ~2–5 nm. The chemical map of iron (Figure 3c) shows enrichment in Fe oxides in the lower portion of the FIB foil. Contrast variations in a STEM picture can generally be explained by a change in sample thickness and/or electronic density of atoms (*Z* contrast). As the thickness of the FIB foil is constant (~100 nm) in this area, contrast of the STEM picture can only be due to changes in the electronic density, hence to chemical variations: Light elements such as carbon appear in dark gray and heavier elements in a brighter gray. Two iron oxides are distinguishable on the STEM picture in Figure 3g. The lower part of the area, in light gray, corresponds to a relic of untransformed starting material: wüstite (Wus). Above, slightly darker, magnetite crystals (Mt) can also be observed. The SAED of magnetite is shown in Figure 3f. XEDS analyses of the dark gray phase in Figure 3g reveal a composition dominated by Fe, C, and O (see Figures 3b and 3c). This Fe-C-O-rich quenched phase can be linked only to the new high-pressure high-temperature phase previously observed by XRD. The Egerton method applied to the EELS data acquired for this phase gives elemental ratios of Fe/C ~ 1.8, Fe/O ~ 0.46, and C/O ~ 0.25 with a low standard deviation (<0.08). When available, ATEM observations indicate that the other "FeO + CO_2" runs display the same quenched phase assemblage as the one observed in run 3. In runs 1 and 2, SAED indicates the additional presence of siderite in the FIB foil, in agreement with in situ X-ray diffraction.

[13] Figure 4 displays electron diffraction patterns obtained along different zone axes of the new Fe-C-O-rich crystalline phase (thin section from run 3). A TEM picture of this crystalline phase is shown in Figure 4a. These patterns and the derived *d* spacings confirm that the quenched structure is different from that observed in situ by XRD prior to temperature and pressure releases. The diffraction pattern in Figure 4b suggests a 6 mm or 3 m lattice symmetry, compatible with cubic or hexagonal space groups, and provides a *d* spacing of 8.14 ± 0.05 Å. The same value of *d* spacing (8.14 ± 0.05 Å) is also observed in other electronic diffraction patterns (e.g., Figures 4c and 4d). We tentatively indexed these diffraction patterns into a hexagonal lattice with $a = 9.40 \pm 0.14$ Å and $c = 12.63 \pm 0.15$ Å or a cubic cell with $a = 11.51 \pm 0.07$ Å. However, neither of these two structures could be used to index all the collected diffraction patterns such as the one presented in Figure 4d. Thus, the exact structure of this quenched Fe-C-O-rich phase remains unresolved. The discrepancies between the data acquired in situ at high pressures and high temperatures and those obtained on the recovered sample might be explained by a structural change occurring on temperature and/or pressure release. As the quenched phase is chemically homogenous with no signs of exsolution, the phase detected at high pressures and high temperatures by in situ XRD likely has the same composition.

[14] NEXAFS data were acquired using STXM at the C K edge on the FIB foils of recovered samples after transformation of FeO + CO_2 at 75 and 70–95 GPa from runs 3 and 4. For both samples, the C K edge spectra reveal a peak at 287.35 eV that can be assigned to $1s \rightarrow \pi^*$ electronic transitions in CO inclusions [*Hitchcock and Brion*, 1980] and a broader peak at about 290.67 eV, which differs from the 290.3 eV peak characteristic of $(CO_3)^{2-}$ groups (Figure 5). Spectra at the Fe $L_{2,3}$ edges, measured in the sample transformed at 75 GPa (run 3), show a higher intensity for the peak at 709.4 eV than for the peak present at 707.8 eV, which indicates that iron is mostly $Fe^{(III)}$ (Figure 5). To clarify this observation and test the influence of $Fe^{(III)}$ on the recombination process, we attempted to directly recombine hematite (Fe_2O_3) and CO_2 at high pressures and high temperatures. This run (run 7) was performed at 88 GPa and 2500 K. As shown in Figure 1d, X-ray diffraction patterns collected in situ reveal the presence of two crystalline phases: the new high-pressure high-temperature Fe-C-O-rich phase and the high-pressure post-perovskite-structured polymorph of Fe_2O_3 described by *Ono et al.* [2004, 2005]. In this run, the high-pressure polymorph of magnetite was not observed.

[15] In order to test the effect of OH content, we also conducted one run with goethite (FeO(OH)) loaded into CO_2 (run 6). Upon compression at room temperature, α-FeO(OH) goethite transformed into the high-pressure polymorph ε-FeO(OH) at pressures above 5 GPa, in agreement with *Gleason et al.* [2008]. X-ray diffraction patterns collected in situ at 2000 K and 55 GPa indicate a mineralogical assemblage similar to the one observed in the FeO-CO_2 system. In addition to the two phases, α-FeO(OH) and ε-FeO(OH) (relics of unreacted starting materials), we can observe diffraction peaks assigned to the high-pressure polymorph of magnetite as well as signatures of the new Fe-C-O high-pressure high-temperature phase previously described in the FeO-CO_2 system (Figure 1c).

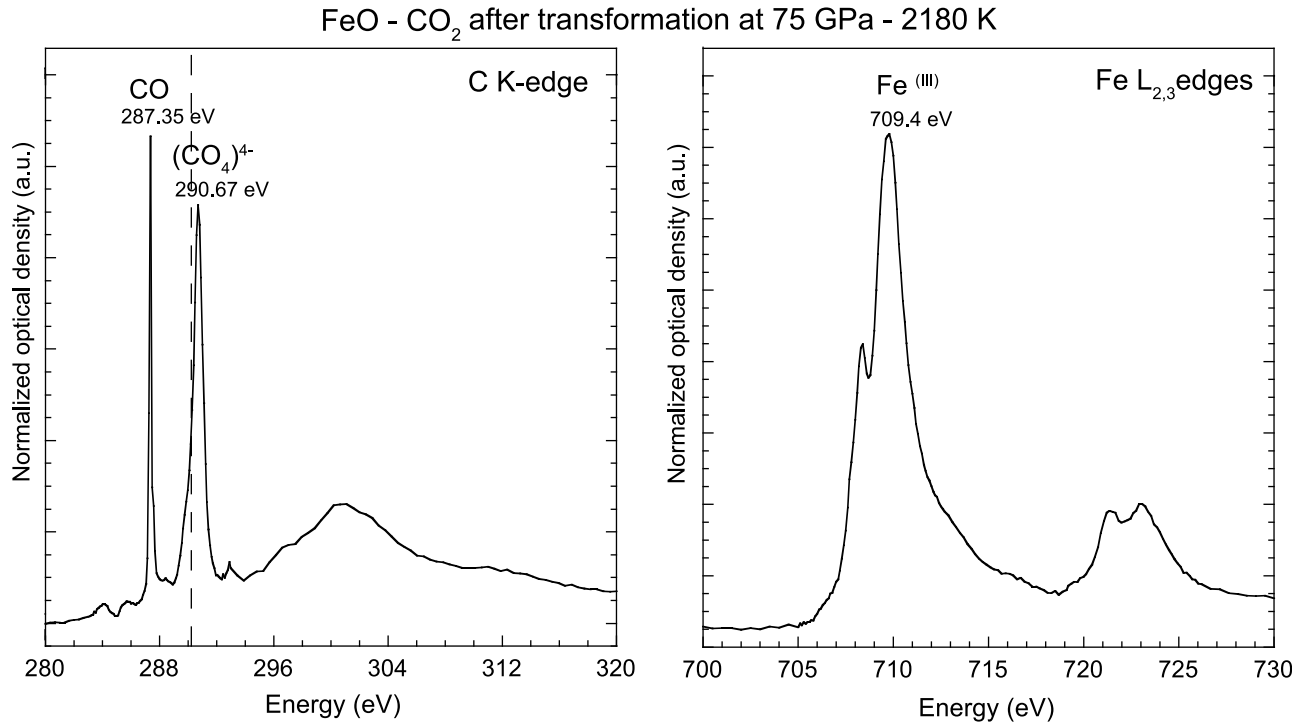

Figure 5. (left) NEXAFS spectrum collected at the C K edge on the quench phase obtained after transformation of FeO + CO_2 at 75 GPa and about 2180 K (run 3). The sharp peak at 287.35 eV is assigned to 1s → π* electronic transitions in CO gas inclusions. The position of the molecular peak of a typical carbonate (290.3 eV) is represented by a dotted line. A broad peak at 290.67 eV is assigned to the presence of $(CO_4)^{4-}$ groups. (right) NEXAFS spectrum collected at the Fe $L_{2,3}$ edges in the same area. The high intensity of the peak at 709.4 eV (relative to the peak at 708 eV) reveals a high $Fe^{(III)}$ content.

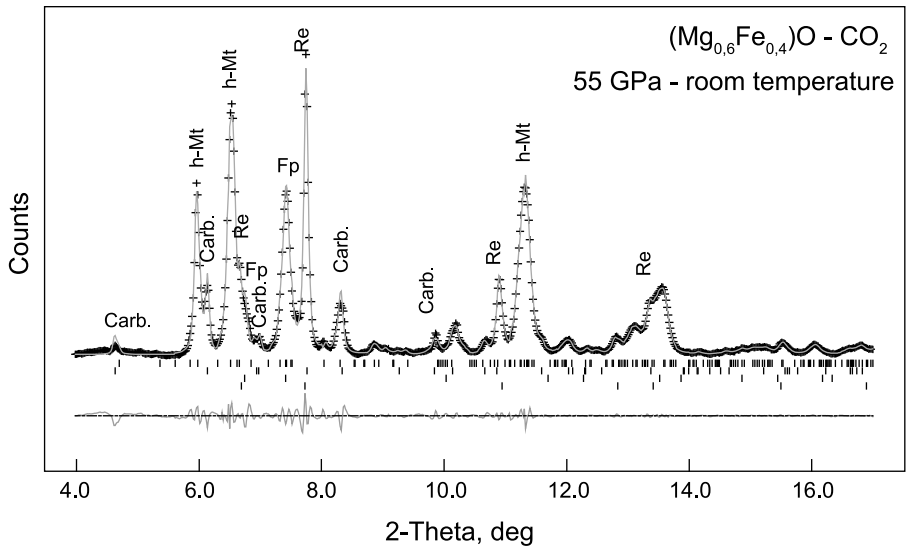

Figure 6. X-ray diffraction pattern collected at 55 GPa and room temperature on sample made from (Mg, Fe)O + CO_2 (run 8). Crosses represent observed diffraction data, and the solid line represents the profile refinement (background subtracted). For the refinement, we used an assemblage of Rhenium (gasket) (Re), (Mg, Fe)O (Fp), (Mg, Fe)CO_3 (Carb.), and the high-pressure polymorph of magnetite (h-Mt). Residuals between observations and fits are shown below.

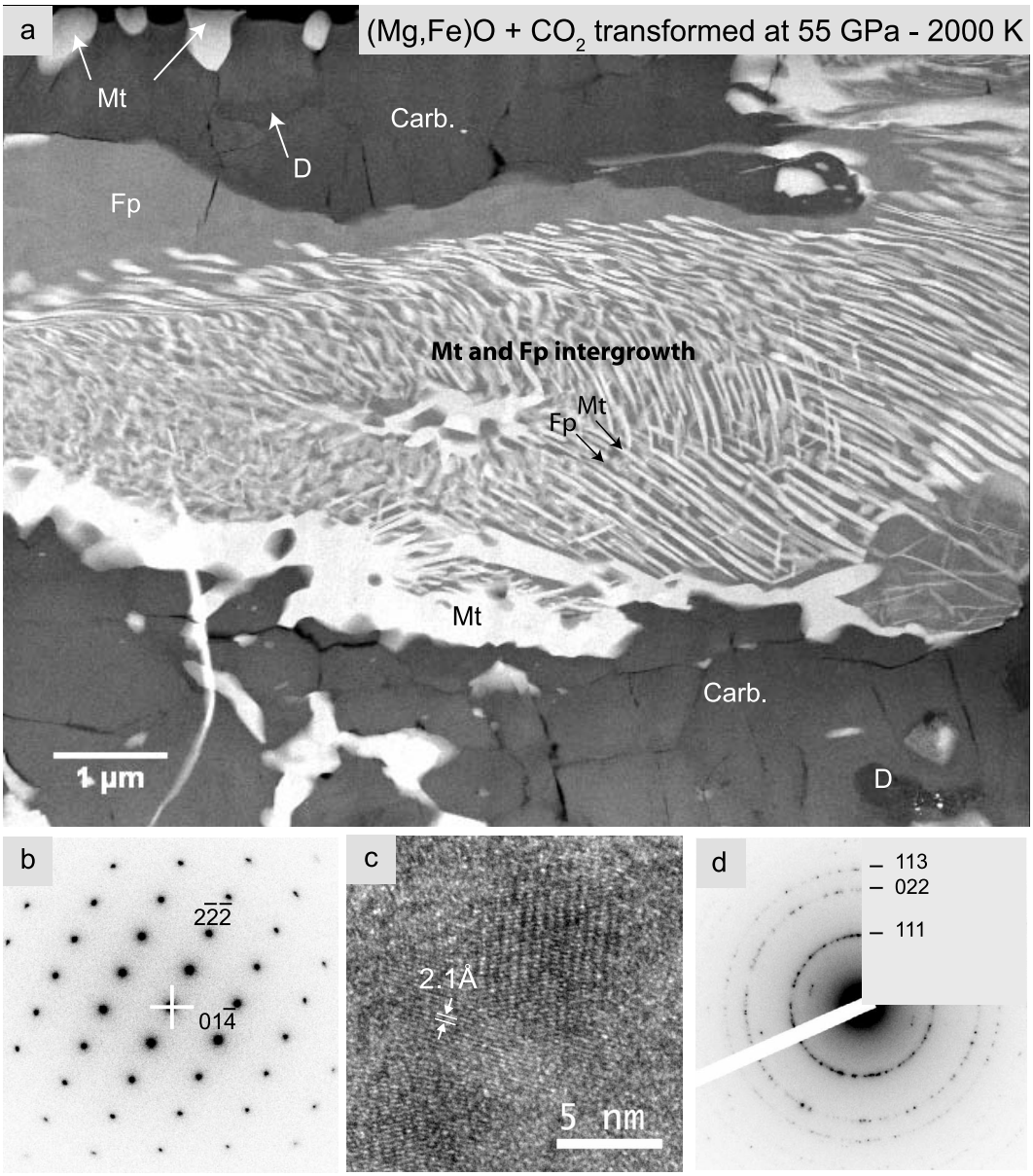

Figure 7. (a) STEM picture of the recovered sample of run 8 (transformation of (Mg,Fe)O + CO_2 at 55 GPa and about 2000 K). Four phases are observed: ferropericlase (Fp), Mg-Fe carbonate (Carb.), magnetite (Mt), and diamond (D). This sample is characterized by a large central area of magnetite-ferropericlase intergrowth and two carbonate and nanodiamond areas. (b) Electron diffraction of (Mg,Fe)CO_3. Distances at 2.78 ± 0.05 and 3.87 ± 0.05 Å are indexed as (0-1-4) and (1-1-1) lattice planes, respectively. (c) High-resolution TEM picture of nanodiamonds. Periodicity of 111 planes at about 2.1 Å intervals is indicated by arrows. (d) Electron diffraction of nanodiamonds. Distances at 1.99 ± 0.05, 1.20 ± 0.05, 1.03 ± 0.05 Å are indexed as (111), (022), and (113) lattice planes of diamond, respectively.

3.2. (Mg, Fe)O-CO_2 Join System

[16] In order to study the effect of Mg on the FeO-CO_2 system, $Mg_{0.6}Fe_{0.4}O$ single crystals were loaded into CO_2 for investigations over a large pressure range, between 55 and 105 GPa (corresponding to depths in the Earth's mantle of about 1350–2350 km). Results are presented below for runs 8–11.

[17] In run 8, a mixture of ($Mg_{0.6}$,$Fe_{0.4}$)O + CO_2 was transformed at 55 GPa and 2000 K. XRD patterns collected in situ at high pressures and high temperatures were indexed as an assemblage of Fe-bearing magnesite, the high-pressure polymorph of magnetite [*Haavik et al.*, 2000], and ferropericlase (Figure 6).

[18] Figure 7 shows ATEM observations obtained on the sample recovered from run 8. The HAADF STEM micrograph in Figure 7a highlights the presence of four different phases: ferropericlase, Mg-Fe carbonate, magnetite, and nanodiamonds. Ferropericlase, identified by both SAED and

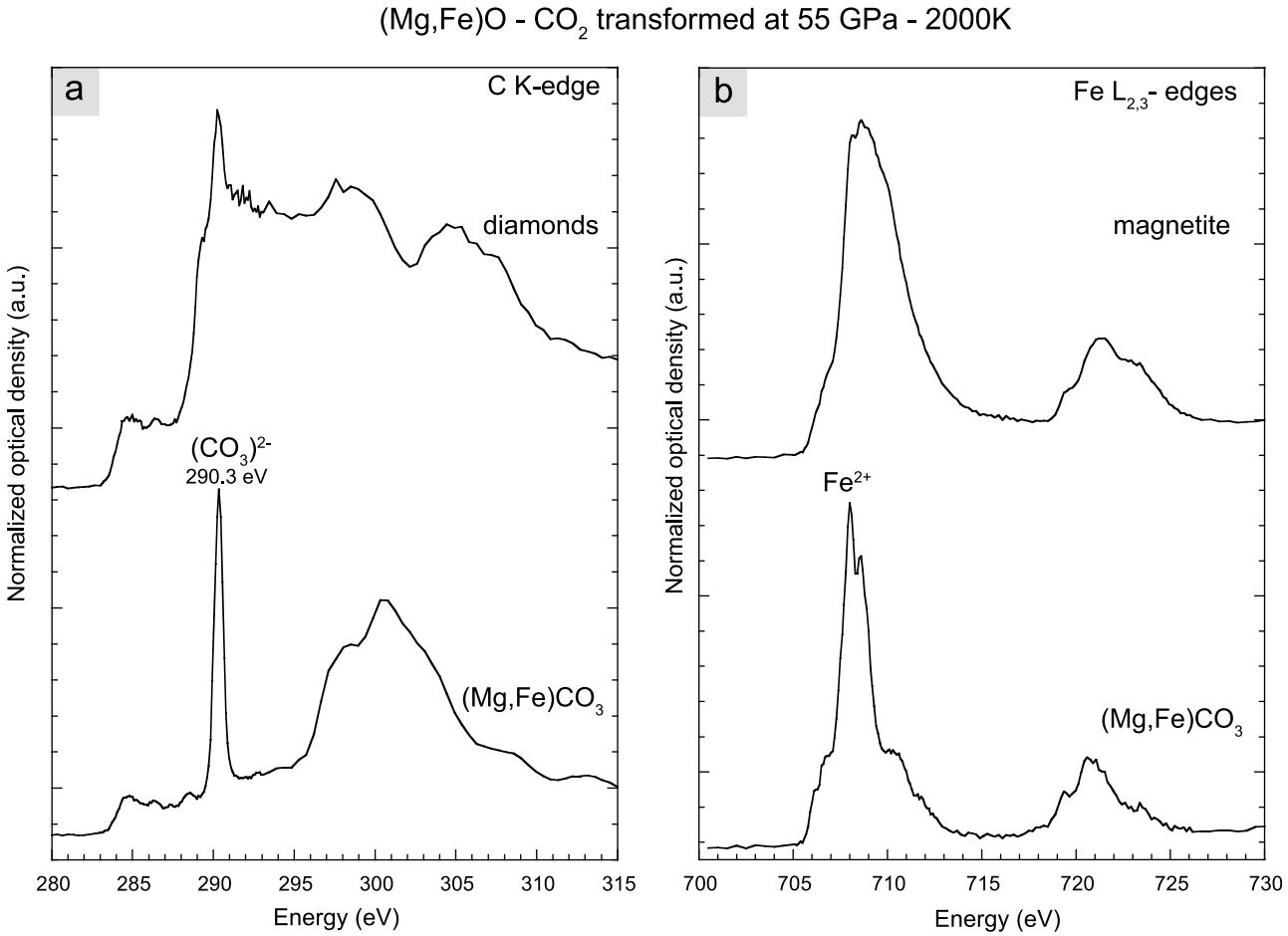

Figure 8. (a) NEXAFS spectrum collected at the C K edge in nanodiamonds and in the carbonate area. The peak at 290.3 eV is assigned to 1s → π* electronic transitions in C = O in planar $(CO_3)^{2-}$ carbonate groups. (b) NEXAFS spectrum collected at the Fe $L_{2,3}$ edge in the carbonate and the magnetite areas. The carbonate spectra show typical features of an $Fe^{(II)}$-bearing phase as expected for a siderite-rich carbonate.

XEDS, is present in the middle of the foil and is interpreted as a relic of unreacted material. The peculiar structure of the sample assemblage is likely due to the single-crystal nature of the starting material that was embedded within CO_2 and heated on both sides. The carbonatation reaction front thus progressed from both sides, but did not affect the central part of the sample. In each of these reaction zones, the starting material is surrounded by Fe-bearing magnesite ((Mg,Fe)CO_3), which was identified by XEDS and SAED (Figure 7b) and confirmed by STXM. Magnetite is also present in the Fe-Mg carbonate areas in association with nanodiamonds. Nanodiamonds in this sample are well crystallized and have sizes of about 10 nm (see the high-resolution TEM micrograph in Figure 7c). Figure 7d displays the SAED pattern of these nanocrystals. In the center of the micrograph, fine intergrowth (∼10 nm scale) of ferropericlase and magnetite is observed. This can be attributed to partial oxidation of ferropericlase, indicating that the redox reaction affected the central area of the sample. The FIB foil cut through the entire thickness of the assemblage is well representative of the whole sample, and XEDS cartography shows no iron concentration gradient as would be expected in the case of a strong Soret effect. XEDS analyses done on the carbonate and on the ferropericlase show Fe/Mg ratios of 0.25 and 0.1, respectively, i.e., lower than the ratio measured in the starting material (Fe/Mg = 0.66). This is a direct consequence of magnetite formation.

[19] STXM analyses of the carbonate phase show typical features of Fe-bearing magnesite. In the NEXAFS spectra collected at the C K edge (Figure 8a), peaks at 290.3 and 298.3 eV can be assigned to 1s → π* electronic transition and the one at 300.5 eV to 1s → σ* electronic transitions in carbonate groups [*Hofer and Golob*, 1987; *Zhou et al.*, 2008]. Spectra collected at the Fe $L_{2,3}$ edges indicate the presence of $Fe^{(II)}$ in the carbonate, as expected for (Mg,Fe)CO_3 (Figure 8b). In agreement with the TEM observations, NEXAFS spectra of the iron oxide at the Fe $L_{2,3}$ edges are characteristic of magnetite [*Paterson and Krivanek*, 1990] (Figure 8b) and spectra collected at the C K edge in the C-rich area are characteristic of diamonds (Figure 8a).

[20] XRD patterns collected in situ at high temperatures and high pressures above 80 GPa differ from those observed at 55 GPa (runs 9, 10, and 11). Reflexions present in these diffraction patterns correspond to neither a carbonate nor to the high-pressure high-temperature phase described in section 3.1, but rather, match the reflexions assigned to a

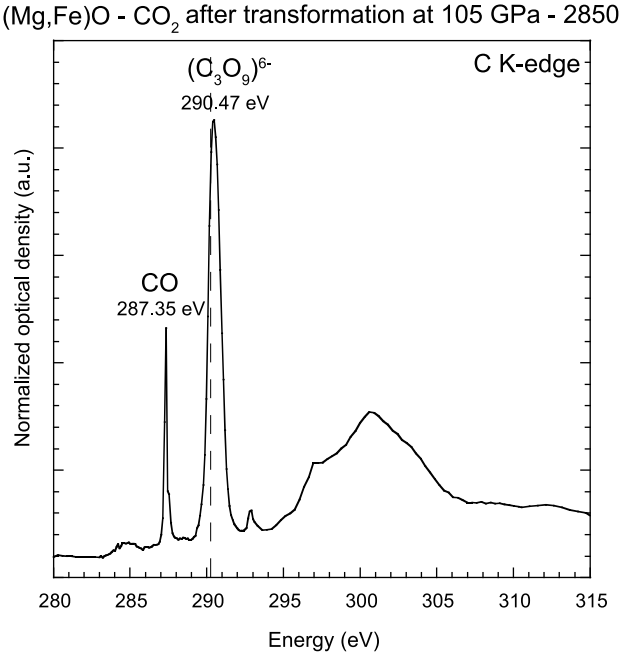

Figure 9. NEXAFS spectrum collected at the C K edge on the high-pressure C-bearing (Mg, Fe)CO_3 phase. The broad peak at 290.47 eV assigned to the presence of $(C_3O_9)^{6-}$ rings of the high-pressure phase [*Boulard et al.*, 2011] is significantly distinct from the main peak assigned to $(CO_3)^{2-}$ groups of low-pressure carbonates (dotted line at 290.3 Å).

high-pressure polymorph of $MgCO_3$ magnesite described by *Boulard et al.* [2011] under similar *P-T* conditions.

[21] ATEM was performed on the two samples recovered from runs 10 and 11, i.e., after transformation of $(Mg_{0.6}Fe_{0.4})O + CO_2$ at 97 GPa and 3650 K and 105 GPa and 2850 K, respectively. Relics of starting materials are still present in the sample transformed at 105 GPa together with the high-pressure polymorph of carbonate described by *Boulard et al.* [2011], magnetite, and nanodiamonds. In the FIB foil extracted from the sample recovered after the transformation of $(Mg_{0.6}Fe_{0.4})O$ loaded into CO_2 at 97 GPa and 3650 K (run 10), only the high-pressure polymorph of carbonate was observed. Fe/Mg ratios determined by XEDS analyses range between 0.5 and 0.8.

[22] STXM analyses were also performed on these two samples. NEXAFS spectra collected at the C K edge on both samples confirmed the characteristic spectroscopic signature observed with lower-energy resolution by EELS in the high-pressure polymorph of (Mg,Fe)CO_3 described by *Boulard et al.* [2011]. When compared with a typical carbonate C K edge spectrum, the main peak is broader and shifted up to 290.47 eV (Figure 9). In agreement with density functional theory (DFT) calculations, this peak is assigned to the presence of $(C_3O_9)^{6-}$ rings of three $(CO_4)^{4-}$ tetrahedral [*Boulard et al.*, 2011]. The smaller peak present at 287.35 eV is assigned to $1s \rightarrow \pi^*$ electronic transition in molecular CO [*Hitchcock and Brion*, 1980]. STXM images were taken at 702, 708.4, and 709.7 eV of the recovered sample of $(Mg_{0.6}Fe_{0.4})O + CO_2$ after transformation at 97 GPa and 3650 K (run 10). In line with previous EELS analyses [*Boulard et al.*, 2011], the comparative analyses of the STXM images indicate a high $Fe^{(III)}/Fe^{(II)}$ ratio in the high-pressure phase of (Mg,Fe)CO_3.

4. Discussion

4.1. A New High-Pressure $Fe_4(CO_4)_3$ Phase

[23] A new high-pressure high-temperature phase was identified in the present experiments carried out in FeO-CO_2 composition. It appears as a minor component in the lower-pressure experiments ($P < 60$ GPa) and becomes the only oxidized C-bearing phase above 60 GPa. XRD patterns clearly show that this new high-pressure high-temperature phase is different from the high-pressure polymorph of magnesite described by *Boulard et al.* [2011]. The best fit of the XRD pattern was obtained with a monoclinic space group. Lattice parameters obtained from LeBail refinements for the different runs are presented in Table 2. Both STXM and EELS spectroscopy show the presence of $Fe^{(III)}$. Considering the measured elemental ratio and the large $Fe^{(III)}$ content, we propose a stoichiometry of $Fe^{(III)}_4(CO_4)_3$ for this phase. This stoichiometry yields ideal elemental ratios of Fe/C = 1.33 and Fe/O = 0.33, slightly lower than those measured on the recovered samples except for C/O (= 0.25). A preferential loss of light elements such as C and O during EELS analysis, which was clearly observed under high beam conditions, can qualitatively explain this discrepancy. We propose two possible lacunar structures for this new phase: (1) a larnite-type (Ca_2SiO_4) or (2) a laihunite- (olivine-) type structure ($Fe^{II}Fe^{III}_2(SiO_4)_2$). Both structures are monoclinic and have cell parameters consistent with those measured by XRD (see Table 2). In contrast with a carbonate structure, carbon in these two structures is present as tetrahedral $(CO_4)^{4-}$ groups. This explains the difference between the NEXAFS analysis on the recovered samples and a typical

Table 2. Lattice Parameters of the New High-Pressure Phase $Fe^{(III)}_4(CO_4)_3$ Measured by In Situ XRD

Run	*P* (GPa)	*T* (K)	a (Å)	b (Å)	c (Å)	β (°)	Volume (Å^3)
1. FeO+CO_2	50	2280	10.16	6.66	6.15	93.04	415.7
2. FeO+CO_2	60	2380	10.19	6.56	6.09	92.88	407.6
3. FeO+CO_2	75	2180	9.95	6.43	6.09	94.28	389.7
4. FeO+CO_2	95	2640	9.83	6.32	5.99	94,24	371.8
5. FeO+CO_2	97	2270	9.88	6.4	5.9	93.14	373.1
6. FeO(OH)+CO_2	55	2000	10.08	6.52	6.17	94.22	405.1
7. Fe_2O_3+CO_2	88	2500	9.94	6.41	5.96	92.73	379.8
Larnite (space group *P* $2_1/n$)			5.48	6.76	9.28	94.55	342.69
Laihunite (space group *P* $2_1/b$)			4.80	10.18	5.80	90	284.0

carbonate C K edge spectrum (see Figure 5). This also implies that the $(CO_4)^{4-}$ groups of the high-pressure high-temperature phase are preserved on quenching at ambient conditions. In line with Pauling's rule predictions, $(CO_4)^{4-}$ groups have been proposed for several C-bearing structures at high pressures. *Iota et al.* [1999] showed, for example, a quartz-like structure at high pressures and high temperatures of CO_2 (phase CO_2-V). In spite of some disagreements over the exact structures, theoretical studies on the stability of magnesite ($MgCO_3$) and calcite ($CaCO_3$) have generally predicted the existence of $(CO_4)^{4-}$ groups in high-pressure carbonate phases [*Skorodumova et al.*, 2005; *Oganov et al.*, 2006, 2008; *Panero and Kabbes*, 2008]. Furthermore, *Ono et al.* [2007] observed experimentally a pyroxene-type $CaCO_3$ at pressures >130 GPa and temperatures >1500 K. Finally, $(CO_4)^{4-}$ group-bearing structures were also proposed in theoretical studies investigating the fate of alkali metal carbonates at high pressures [*Čančarevič et al.*, 2006, 2007]. The $Fe^{(III)}$-rich composition can be related to the formation of nanodiamonds, which are systematically observed in contact with this high-pressure high-temperature phase. It must be noted that CO inclusions are also observed in the recovered samples. It is not known yet whether CO was formed at high pressure and temperature or on decompression. It is worth noticing that CO has never been observed or predicted in the evolution of CO_2 at high pressures and temperatures. Rather, a direct breakdown of CO_2 into $C + O_2$ was observed [*Litasov et al.*, 2011] or calculated [*Oganov et al.*, 2008]. In the present study, if CO was formed at high pressures and high temperatures, it means that evolution of CO_2 in the presence of FeO is different form that in a pure CO_2 composition. We thus suggest that $Fe^{(II)}$ oxidation into $Fe^{(III)}$ is balanced by the reduction of CO_2 into C or possibly CO. Thus, the chemical reaction for the formation of this new phase can be written as follows:

$$(R1) \qquad 4FeO + 4CO2 \rightarrow Fe4(CO4)3 + C$$

or

$$(R2) \qquad 4FeO + 5CO2 - > Fe4(CO4)3 + 2CO.$$

In the same areas, a high-pressure polymorph of magnetite is formed as well, following the redox mass balance:

$$(R3) \qquad 6FeO + CO_2 = 2Fe_3O_4 + C.$$

4.2. Stability of Carbon-Bearing Phases at Lower Mantle Conditions

[24] Several experimental studies have investigated carbonate stability during subduction down to the lower mantle. There is no consensus about the exact location of the solidus of carbonates at upper mantle conditions. It thus remains unclear whether carbonates can be preserved while migrating through the upper mantle and the transition zone. The experimental study of *Hammouda* [2003] predicts that carbon cannot be recycled below 300 km in the mantle because of removal from the subducting plate by melting or decarbonatation reactions. However, other studies such as those of *Katsura and Ito* [1990], *Poli and Schmidt* [2002], *Dasgupta et al.* [2004], *Yaxley and Brey* [2004], and *Gorman et al.* [2006] have argued that a large part of the carbon can be preserved in the subducting lithosphere, particularly along cool or intermediate thermal subduction paths. Although the melting temperature of a volatile-bearing system is lower than that of a volatile-free system, this melting temperature depression seems to be not enough to melt all carbonates from subducting plates: Indeed, carbonated eclogite solidus and carbonated peridotite solidus are found close to the average mantle geotherm for pressures up to 32 GPa [*Ghosh et al.*, 2009; *Litasov and Ohtani*, 2009, 2010]. Thus, no melting of carbonated peridotite or carbonated eclogite is expected to happen during subduction and carbonates could be recycled in the deep mantle. Our experiments were done as a continuation of this hypothesis by testing carbonate stability at lower mantle conditions. As presented in Figure 10, most of our experiments were performed at temperatures up to 200 K close to or above the adiabatic mantle geotherm and therefore at higher temperatures than in any subduction *P-T* path. The experiments detailed above unambiguously show the formation of $FeCO_3$ and $(Mg,Fe)CO_3$ carbonates at pressures below 40 and 80 GPa, respectively (see Figure 10) as a result of the recombination of oxides $FeO + CO_2$ and $(Mg,Fe)O + CO_2$. This indicates that carbonates are thermodynamically more stable than oxides under *P-T* conditions corresponding to the lower mantle geotherm. To our knowledge, there are no data documenting pressure-induced decomposition of $FeCO_3$ into oxides at high pressure, while $MgCO_3$ decomposition has already been investigated [*Redfern et al.*, 1993; *Fiquet et al.*, 2002]. The experimental conditions and the calculated $MgCO_3$ decomposition line ($MgCO_3 \rightarrow MgO + CO_2$) from *Fiquet et al.* [2002] are shown in Figure 10. All samples studied here, except two, have been synthesized at pressures and temperatures beneath this decomposition curve, in line with the observation of syntheses of carbonates in our experiments. One sample was heated at a temperature above the extrapolated decomposition line of magnesite (97 GPa–3700 K), and still the recombination of oxides into the high-pressure polymorph of Fe-bearing magnesite was documented. This observation suggests that this high-pressure polymorph of magnesite described by *Boulard et al.* [2011] is thermally more stable than magnesite. The next step for understanding the stability of oxidized forms of carbon in the lower mantle will be to investigate their stability in presence of a silicate phase. *Seto et al.* [2008] have suggested that chemical interactions between carbonates and silicates could alter the stability field of carbonates according to the reaction $MgCO_3 + SiO_2 \rightarrow MgSiO_3 + CO_2$. This reaction was later confirmed by the experimental study of *Litasov et al.* [2008]. As shown in Figure 10, the location of this reaction in *P-T* space requires that further experimental studies assess the role of carbonate-silicate reactions at high temperatures and high pressures on the actual stability of oxidized forms of carbon in the Earth's lower mantle.

[25] Considering reactions (R1) and (R2), the Fe/CO_2 ratio in the starting material seems to be a factor of importance. Formation of the high-pressure high-temperature phase $Fe_4(CO_4)_3$ may require a large amount of CO_2. Although we did not specifically control the initial Fe/CO_2 ratio in our

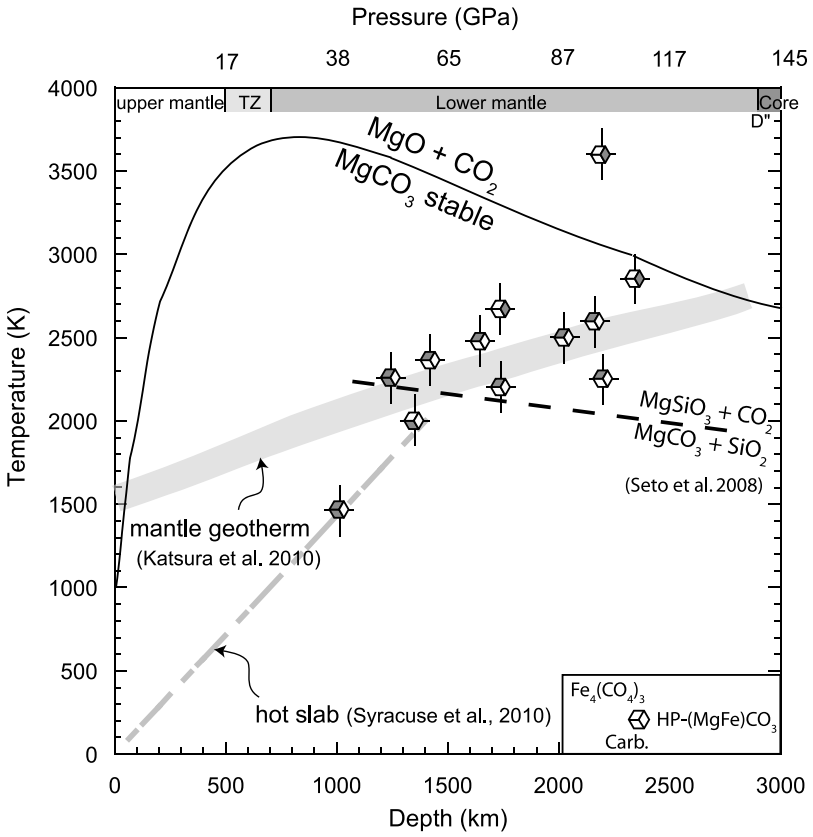

Figure 10. Tentative location of the experiments in a temperature-depth diagram. Sectors of hexagons represent the phases present (abbreviations as in Table 1).The adiabatic mantle geotherm predicted by *Katsura et al.* [2010] and the hot slab geotherm determined by *Syracuse et al.* [2010] are represented in gray. The decomposition line of magnesite predicted by *Fiquet et al.* [2002] and the reaction curve $MgCO_3 + SiO_2 \rightarrow MgSiO_3 + CO_2$ determined by *Seto et al.* [2008] are shown for comparison.

experiments, it was smaller than a realistic ratio under lower mantle conditions. Further studies on the effect of lower amounts of CO_2 on the stability field of these high-pressure phases are thus needed.

[26] The initial amount of $Fe^{(II)}$ is also of significant importance since the nature of the high-pressure phase depends on the $Fe^{(II)}$ content. The new phase $Fe_4(CO_4)_3$ was observed when using FeO, Fe_2O_3, or FeO(OH) oxide starting materials and for pressures and temperatures above 40 GPa and 1500 K, respectively, while the phase described by *Boulard et al.* [2011] was observed when combining $(Mg_{0.4}, Fe_{0.6})O$ and MgO oxides and CO_2 experiments at conditions above 80 GPa and 2000 K. The Fe/Mg ratio affects the phase boundaries and the high-pressure polymorphs, in agreement with previous reports about various carbonate compositions [see *Santillán and Williams*, 2004].

[27] Although $Fe^{(II)}$ is the dominant species of iron in the upper mantle ($Fe^{(III)}/\Sigma Fe < 0.03$) [e.g., *Canil and O'Neill*, 1996], the amount of ferric iron is predicted to be much more important in the lower mantle ($Fe^{(III)}/\Sigma Fe \geq 0.6$) as silicate perovskite incorporates a large amount of $Fe^{(III)}$ [*Frost et al.*, 2004]. The experiment on Fe_2O_3-CO_2 transformed at 88 GPa confirms that the new phase $Fe_4(CO_4)_3$ forms, even when starting directly from a $Fe^{(III)}$-bearing oxide. Obviously, in this case, no redox reaction took place, which explains why neither hematite nor diamonds were observed in the sample. Recombination of oxides occurred according to

$$2Fe_2O_3 + 3CO_2 \rightarrow Fe_4(CO_4)_3. \quad \text{(R4)}$$

This observation reinforces the notion of incorporation of a large amount of $Fe^{(III)}$ in the new high-pressure high-temperature phase.

[28] *Peacock* [1990] estimated the amount of water transported by subducting slabs into the mantle to be at least 8.7×10^{11} kg/year. The flux of water outgassing from the mantle through magmatism is much lower and is estimated at 2×10^{11} kg/year [*Peacock*, 1990]. This discrepancy may result from hydration of the mantle wedge overlying the subducting slab [*Peacock*, 1990]. Alternatively, *Ohtani* [2005] proposed the misbalance to be linked to transport of water into the deep mantle. Usually dehydration is admitted to occur in the upper part of the mantle. However, in cold subducting slabs, some water may be transported into the transition zone and the lower mantle [e.g., *Ringwood and Major*, 1967; *Ohtani*, 2005; *Inoue et al.*, 2010]. Thus, it was also important to check whether the new phase could still be stable in hydrous systems. Our experiment, carried out on a simple hydrated starting material (FeO(OH) loaded in pure CO_2), showed

formation of the same high-pressure high-temperature phase $Fe_4(CO_4)_3$ at 55 GPa, in agreement with experiments on H_2O-free systems.

[29] In the Earth's lower mantle, the capacity of perovskite $(Mg,Fe)(Al,Si)O_3$ to incorporate a large amount of $Fe^{(III)}$ is likely balanced by a corresponding amount of metallic iron, which could buffer the oxygen fugacity in the bulk lower mantle at metal saturation [e.g., *Frost et al.*, 2004]. Therefore, the general assumption is that carbonates in the lower mantle would be replaced by reduced forms of carbon. Carbon would then be stored as diamond, carbides, or an alloying element in metals [e.g., *Dasgupta and Hirschmann*, 2010; *Rohrbach and Schmidt*, 2011]. However, locally, in oxidized areas such as subducting lithospheric plates, carbonates may remain stable. In the present study, reduced and oxidized forms of carbon were observed together in the recovered samples. At first, this coexistence may be seen as evidence for local disequilibrium. However, this seems unlikely given the close relationship between reduced and oxidized species (see Figures 3 and 7) and the heating duration of about 2 h used in our experiments. Moreover, ATEM analyses on the recovered sample show no compositional gradients in the phases, further suggesting that equilibrium was achieved. This is also reinforced by the fact that experiments carried out with $(Mg,Fe)CO_3$ as starting material [*Boulard et al.*, 2011] led to the same mineralogical assemblage than in the $(Mg,Fe)O + CO_2$ experiments described here.

[30] Therefore, our experiments show the coexistence of carbonates or their high-pressure polymorphs with nanodiamonds in the recovered samples. Even though more data at different oxygen fugacities and different $Fe^{(II)}/CO_2$ ratios are necessary, our study indicates that carbon could be stored in the lower mantle as an assemblage of diamonds and either Fe-bearing magnesite or one of the new C-bearing high-pressure phases described here. This proposition differs from the models that have been proposed so far, which usually support the idea of carbon being stored either as carbonates in the more oxidized part of the lower mantle [*Wood et al.*, 1996] or as diamonds in more reduced conditions [*McCammon*, 2006; *Frost and McCammon*, 2008]. The possibility for C-reduced phases to coexist with C-oxidized phases has recently been proposed for upper mantle assemblages [*Stagno and Frost*, 2010]. We suggest extending this possibility to deep mantle conditions in areas initially made of large amounts of carbonates, for instance, in a subducting slab. The formation of diamonds in the lower mantle is usually ascribed to the reduction of carbon from an oxidized C-bearing fluid that is transferred to a reduced environment [*Deines*, 2002; *Haggerty*, 1986]. Provided that the reactions described in this paper are representative of mantle conditions, our results support an alternative mechanism to form diamonds from an initially single homogenous $Fe^{(II)}$-bearing carbonate phase brought at the appropriate pressure and temperature conditions.

[31] **Acknowledgments.** The authors thank P. Munsch, G. Le Marchand, and H. Ozawa for their help with experiments and cell loadings. M. Cabie, D. Troadec, and I. Machouk are acknowledged for their help with FIB sample preparation. The focused ion beam (FIB) and scanning electron microscopy (SEM) facility of the Institut de Minéralogie et de Physique des Milieux Condensés is supported by Région Ile de France grant SESAME 2006 N°I-07-593/R, INSU-CNRS, INP-CNRS, University Pierre et Marie Curie-Paris 6, and by the French National Research Agency (ANR) grant ANR-07-BLAN-0124-01. A.C. acknowledges financial support from the PNP-INSU program and the European Research Council under European Research Community's seven framework program (FP7/2007–2013)/ERC grant agreement 207467. The ALS-MES beamline 11.0.2 is supported by the Director, Office of Science, Office of Basic Energy Sciences, Division of Chemical Sciences, Geosciences, and Biosciences and Materials Sciences Division of the U.S. Department of Energy at the Lawrence Berkeley National Laboratory. The CLS 10ID-1 STXM beamline is supported by NSERC, CIHR, NRC, and the University of Saskatchewan. We thank Tolek Tylisczak, the beamline scientist on 11.0.2, and Chithra Karunakaran and Jian Wang, the beamline scientists on 10ID-1. Gordon E. Brown Jr. is thanked for providing some beam time on 11.0.2. The two reviewers and the editor are warmly thanked for their help in strongly improving the quality of the manuscript.

References

Alt, J. C., and D. A. H. Teagle (1999), The uptake of carbon during alteration of ocean crust, *Geochim. Cosmochim. Acta*, *63*(10), 1527–1535, doi:10.1016/S0016-7037(99)00123-4.

Auzende, A. L., J. Badro, F. J. Ryerson, P. K. Weber, S. J. Fallon, A. Addad, J. Siebert, and G. Fiquet (2008), Element partitioning between magnesium silicate perovskite and ferropericlase: New insights into bulk lower-mantle geochemistry, *Earth Planet. Sci. Lett.*, *269*(1–2), 164–174, doi:10.1016/j.epsl.2008.02.001.

Benedetti, L. R., and P. Loubeyre (2004), Temperature gradients, wavelength-dependent emissivity, and accuracy of high and very-high temperatures measured in the laser-heated diamond cell, *High Pressure Res.*, *24*(4), 423–445, doi:10.1080/08957950412331331718.

Benzerara, K., T. H. Yoon, T. Tyliszczak, B. Constantz, A. M. Spormann, and G. E. Brown (2004), Scanning transmission X-ray microscopy study of microbial calcification, *Geobiology*, *2*(4), 249–259, doi:10.1111/j.1472-4677.2004.00039.x.

Biellmann, C., P. Gillet, F. Guyot, J. Peyronneau, and B. Reynard (1993), Experimental evidence for carbonate stability in the Earth's lower mantle, *Earth Planet. Sci. Lett.*, *118*(1–4), 31–41, doi:10.1016/0012-821X(93)90157-5.

Boulard, E., A. Gloter, A. Corgne, D. Antonangeli, A. L. Auzende, J. P. Perrillat, F. Guyot, and G. Fiquet (2011), New host for carbon in the deep Earth, *Proc. Natl. Acad. Sci. U. S. A.*, *108*(13), 5184–5187, doi:10.1073/pnas.1016934108.

Brenker, F. E., C. Vollmer, L. Vincze, B. Vekemans, A. Szymanski, K. Janssens, I. Szaloki, L. Nasdala, W. Joswig, and F. Kaminsky (2007), Carbonates from the lower part of transition zone or even the lower mantle, *Earth Planet. Sci. Lett.*, *260*(1–2), 1–9, doi:10.1016/j.epsl.2007.02.038.

Čančarevič, Ž. P., J. C. Schön, and M. Jansen (2006), Alkali metal carbonates at high pressure, *Z. Anorg. Allge. Chem.*, *632*, 1437–1448, doi:10.1002/zaac.200600068.

Čančarevič, Ž. P., J. C. Schön, and M. Jansen (2007), Possible existence of alkali metal orthocarbonates at high pressure, *Chem. Eur. J.*, *13*, 7330–7348, doi:10.1002/chem.200601637.

Canil, D. (1990), Experimental study bearing on the absence of carbonate in mantle-derived xenoliths, *Geology*, *18*(10), 1011–1013, doi:10.1130/0091-7613(1990)018<1011:ESBOTA>2.3.CO;2.

Canil, D., and H. S. C. O'Neill (1996), Distribution of ferric iron in some upper-mantle assemblages, *J. Petrol.*, *37*(3), 609–635, doi:10.1093/petrology/37.3.609.

Dasgupta, R., and M. M. Hirschmann (2010), The deep carbon cycle and melting in Earth's interior, *Earth Planet. Sci. Lett.*, *298*(1–2), 1–13, doi:10.1016/j.epsl.2010.06.039.

Dasgupta, R., M. M. Hirschmann, and A. C. Withers (2004), Deep global cycling of carbon constrained by the solidus of anhydrous, carbonated eclogite under upper mantle conditions, *Earth Planet. Sci. Lett.*, *227*(1–2), 73–85, doi:10.1016/j.epsl.2004.08.004.

Deines, P. (2002), The carbon isotope geochemistry of mantle xenoliths, *Earth Sci. Rev.*, *58*(3–4), 247–278, doi:10.1016/S0012-8252(02)00064-8.

Egerton, R. F. (Ed.) (1996), *Electron Energy-Loss Spectroscopy in The Electron Microscope*, 2nd ed., Plenum, New York.

Fei, Y. W., L. Zhang, A. Corgne, H. Watson, A. Ricolleau, Y. Meng, and V. Prakapenka (2007), Spin transition and equations of state of (Mg, Fe)O solid solutions, *Geophys. Res. Lett.*, *34*, L17307, doi:10.1029/2007GL030712.

Fiquet, G., F. Guyot, M. Kunz, J. Matas, D. Andrault, and M. Hanfland (2002), Structural refinements of magnesite at very high pressure, *Am. Mineral.*, *87*(8–9), 1261–1265.

Fiquet, G., A. L. Auzende, J. Siebert, A. Corgne, H. Bureau, H. Ozawa, and G. Garbarino (2010), Melting of peridotite to 140 gigapascals, *Science*, *329*(5998), 1516–1518, doi:10.1126/science.1192448.

Frost, D. J., and C. A. McCammon (2008), The redox state of Earth's mantle, *Annu. Rev. Earth Planet. Sci.*, *36*, 389–420, doi:10.1146/annurev.earth.36.031207.124322.

Frost, D. J., C. Liebske, F. Langenhorst, C. A. McCammon, R. G. Tronnes, and D. C. Rubie (2004), Experimental evidence for the existence of iron-rich metal in the Earth's lower mantle, *Nature*, *428*(6981), 409–412, doi:10.1038/nature02413.

Ghosh, S., E. Ohtani, K. D. Litasov, and H. Terasaki (2009), Solidus of carbonated peridotite from 10 to 20 GPa and origin of magnesiocarbonatite melt in the Earth's deep mantle, *Chem. Geol.*, *262*, 17–28, doi:10.1016/j.chemgeo.2008.12.030.

Gleason, A. E., R. Jeanloz, and M. Kunz (2008), Pressure-temperature stability studies of FeOOH using X-ray diffraction, *Am. Mineral.*, *93*(11–12), 1882–1885, doi:10.2138/am.2008.2942.

Gorman, P. J., D. M. Kerrick, and J. A. D. Connolly (2006), Modeling open system metamorphic decarbonation of subducting slabs, *Geochem. Geophys. Geosyst.*, *7*, Q04007, doi:10.1029/2005GC001125.

Haavik, C., S. Stolen, H. Fjellvag, M. Hanfland, and D. Hausermann (2000), Equation of state of magnetite and its high-pressure modification: Thermodynamics of the Fe-O system at high pressure, *Am. Mineral.*, *85*(3–4), 514–523.

Haggerty, S. E. (1986), Diamond genesis in a multiply-constrained model, *Nature*, *320*(6057), 34–38, doi:10.1038/320034a0.

Hammersley, A. P., S. O. Svensson, M. Hanfland, A. N. Fitch, and D. Hausermann (1996), Two-dimensional detector software: From real detector to idealised image or two-theta scan, *High Pressure Res.*, *14*(4–6), 235–248, doi:10.1080/08957959608201408.

Hammouda, T. (2003), High-pressure melting of carbonated eclogite and experimental constraints on carbon recycling and storage in the mantle, *Earth Planet. Sci. Lett.*, *214*(1–2), 357–368, doi:10.1016/S0012-821X(03)00361-3.

Hitchcock, A. P., and C. E. Brion (1980), *K*-shell excitation spectra of CO, N_2 and O_2, *J. Electron Spectrosc. Relat. Phenom.*, *18*(1), 1–21, doi:10.1016/0368-2048(80)80001-6.

Hofer, F., and P. Golob (1987), New examples for near-edge fine structures in electron energy loss spectroscopy, *Ultramicroscopy*, *21*(4), 379–383, doi:10.1016/0304-3991(87)90036-2.

Inoue, T., T. Wada, R. Sasaki, and H. Yurimoto (2010), Water partitioning in the Earth's mantle, *Phys. Earth Planet. Inter.*, *183*(1–2), 245–251, doi:10.1016/j.pepi.2010.08.003.

Iota, V., C. S. Yoo, and H. Cynn (1999), Quartzlike carbon dioxide: An optically nonlinear extended solid at high pressures and temperatures, *Science*, *283*(5407), 1510–1513, doi:10.1126/science.283.5407.1510.

Isshiki, M., T. Irifune, K. Hirose, S. Ono, Y. Ohishi, T. Watanuki, E. Nishibori, M. Takata, and M. Sakata (2004), Stability of magnesite and its high-pressure form in the lowermost mantle, *Nature*, *427*(6969), 60–63, doi:10.1038/nature02181.

Javoy, M. (1997), The major volatile elements of the Earth: Their origin, behavior, and fate, *Geophys. Res. Lett.*, *24*(2), 177–180, doi:10.1029/96GL03931.

Katsura, T., and E. Ito (1990), Melting and subsolidus phase relations in the $MgSiO_3$–$MgCO_3$ system at high pressures: Implications to evolution of the Earth's atmosphere, *Earth Planet. Sci. Lett.*, *99*, 110–117, doi:10.1016/0012-821X(90)90074-8.

Katsura, T., Y. Tsuchida, E. Ito, T. Yagi, W. Utsumi, and S. Akimoto (1991), Stability of magnesite under the lower mantle conditions, *Proc. Jpn. Acad., Ser. B*, *67*(4), 57–60, doi:10.2183/pjab.67.57.

Katsura, T., A. Yoneda, D. Yamazaki, T. Yoshino, and E. Ito (2010), Adiabatic temperature profile in the mantle, *Phys. Earth Planet. Inter.*, *183*, 212–218, doi:10.1016/j.pepi.2010.07.001.

Keppler, H., M. Wiedenbeck, and S. S. Shcheka (2003), Carbon solubility in olivine and the mode of carbon storage in the Earth's mantle, *Nature*, *424*(6947), 414–416, doi:10.1038/nature01828.

Larson, A. C., and R. B. Von Dreele (1994), General structure analysis system (GSAS), *Rep. LA (U. S.) LAUR, 86*, Los Alamos Natl. Lab., Los Alamos, N. M.

Lécuyer, C., L. Simon, and F. Guyot (2000), Comparison of carbon, nitrogen and water budgets on Venus and the Earth, *Earth Planet. Sci. Lett.*, *181*(1–2), 33–40, doi:10.1016/S0012-821X(00)00195-3.

Litasov, K., and E. Ohtani (2009), Solidus and phase relations of carbonated peridotite in the system CaO–Al_2O_3–MgO–SiO_2–Na_2O–CO_2 to the lower mantle depths, *Phys. Earth Planet. Inter.*, *177*, 46–58, doi:10.1016/j.pepi.2009.07.008.

Litasov, K., and E. Ohtani (2010), The solidus of carbonated eclogite in the system CaO-Al_2O_3-MgO-SiO_2-Na_2O-CO_2 to 32 GPa and carbonatite liquid in the deep mantle, *Earth Planet. Sci. Lett.*, *295*(1–2), 115–126, doi:10.1016/j.epsl.2010.03.030.

Litasov, K., Y. Fei, E. Ohtani, T. Kuribayashi, and K. Funakoshi (2008), Thermal equation of state of magnesite to 32 GPa and 2073 K, *Phys. Earth Planet. Inter.*, *168*, 191–203, doi:10.1016/j.pepi.2008.06.018.

Litasov, K., A. F. Goncharov, and R. J. Hemley (2011), Crossover from melting to dissociation of CO_2 under pressure: Implications for the lower mantle, *Earth Planet. Sci. Lett.*, *309*(3–4), 318–323, doi:10.1016/j.epsl.2011.07.006.

Ma, Y., C. T. Chen, G. Meigs, K. Randall, and F. Sette (1991), High-resolution *K*-shell photoabsorption measurements of simple molecules, *Phys. Rev. A*, *44*(3), 1848–1858, doi:10.1103/PhysRevA.44.1848.

Macpherson, C. G., D. R. Hilton, and K. Hammerschmidt (2010), No slab-derived CO_2 in Mariana Trough back-arc basalts: Implications for carbon subduction and for temporary storage of CO_2 beneath slow spreading ridges, *Geochem. Geophys. Geosyst.*, *11*, Q11007, doi:10.1029/2010GC003293.

Mao, H. K., J. Xu, and P. M. Bell (1986), Calibration of the ruby pressure gauge to 800-kbar under quasi-hydrostatic conditions, *J. Geophys. Res.*, *91*(B5), 4673–4676, doi:10.1029/JB09iB05p04673.

McCammon, C. (2006), Microscopic properties to macroscopic behaviour: The influence of iron electronic state, *J. Mineral. Petrol. Sci.*, *101*(3), 130–144, doi:10.2465/jmps.101.130.

Mezouar, M., et al. (2005), Development of a new state-of-the-art beamline optimized for monochromatic single-crystal and powder X-ray diffraction under extreme conditions at the ESRF, *J. Synchrotron Radiat.*, *12*, 659–664, doi:10.1107/S0909049505023216.

Miot, J., K. Benzerara, G. Morin, S. Bernard, O. Beyssac, E. Larquet, A. Kappler, and F. Guyot (2009), Transformation of vivianite by anaerobic nitrate-reducing iron-oxidizing bacteria, *Geobiology*, *7*(3), 373–384, doi:10.1111/j.1472-4669.2009.00203.x.

Molina, J. F., and S. Poli (2000), Carbonate stability and fluid composition in subducted oceanic crust: An experimental study on H_2O-CO_2-bearing basalts, *Earth Planet. Sci. Lett.*, *176*(3–4), 295–310, doi:10.1016/S0012-821X(00)00021-2.

Morard, G., D. Andrault, N. Guignot, C. Sanloup, M. Mezouar, S. Petitgirard, and G. Fiquet (2008), In situ determination of Fe-Fe_3S phase diagram and liquid structural properties up to 65 GPa, *Earth Planet. Sci. Lett.*, *272*(3–4), 620–626, doi:10.1016/j.epsl.2008.05.028.

Oganov, A. R., C. W. Glass, and S. Ono (2006), High-pressure phases of CaCO3: Crystal structure prediction and experiment, *Earth Planet. Sci. Lett.*, *241*, 95–103.

Oganov, A. R., S. Ono, Y. M. Ma, C. W. Glass, and A. Garcia (2008), Novel high-pressure structures of $MgCO_3$, $CaCO_3$ and CO_2 and their role in Earth's lower mantle, *Earth Planet. Sci. Lett.*, *273*(1–2), 38–47, doi:10.1016/j.epsl.2008.06.005.

Ohtani, E. (2005), Water in the mantle, *Elements*, *1*(1), 25–30, doi:10.2113/gselements.1.1.25.

Ono, S., T. Kikegawa, and Y. Ohishi (2004), High-pressure phase transition of hematite, Fe_2O_3, *J. Phys. Chem. Solids*, *65*(8–9), 1527–1530, doi:10.1016/j.jpcs.2003.11.042.

Ono, S., K. Funakoshi, Y. Ohishi, and E. Takahashi (2005), In situ x-ray observation of the phase transformation of Fe_2O_3, *J. Phys. Condens. Matter*, *17*(2), 269–276, doi:10.1088/0953-8984/17/2/003.

Ono, S., T. Kikegawa, and Y. Ohishi (2007), High-pressure transition of $CaCO_3$, *Am. Mineral.*, *92*, 1246–1249, doi:10.2138/am.2007.2649.

Panero, W. R., and J. E. Kabbes (2008), Mantle-wide sequestration of carbon in silicates and the structure of magnesite II, *Geophys. Res. Lett.*, *35*, L14307, doi:10.1029/2008GL034442.

Paterson, J. H., and O. L. Krivanek (1990), Elnes of 3d transition metal oxides. 2. Variations with oxidation state and crystal structure, *Ultramicroscopy*, *32*(4), 319–325, doi:10.1016/0304-3991(90)90078-Z.

Peacock, S. M. (1990), Fluid processes in subduction zones, *Science*, *248*(4953), 329–337, doi:10.1126/science.248.4953.329.

Poli, S., and M. W. Schmidt (2002), Petrology of subducted slabs, *Annu. Rev. Earth Planet. Sci.*, *30*, 207–235, doi:10.1146/annurev.earth.30.091201.140550.

Redfern, S. A. T., B. J. Wood, and C. M. B. Henderson (1993), Static compressibility of magnesite to 20 GPa: Implications for $MgCO_3$ in the lower mantle, *Geophys. Res. Lett.*, *20*(19), 2099–2102, doi:10.1029/93GL02507.

Ringwood, A. E., and A. Major (1967), High pressure reconnaissance investigations in system Mg_2SiO_4-MgO-H_2O, *Earth Planet. Sci. Lett.*, *2*(2), 130–133, doi:10.1016/0012-821X(67)90114-8.

Rohrbach, A., and M. W. Schmidt (2011), Redox freezing and melting in the Earth's deep mantle resulting from carbon-iron redox coupling, *Nature*, *472*(7342), 209–212, doi:10.1038/nature09899.

Santillán, J., and Q. Williams (2004), A high-pressure infrared and X-ray study of $FeCO_3$ and $MnCO_3$: Comparison with $CaMg(CO_3)_2$-dolomite, *Phys. Earth Planet. Inter.*, *143–144*, 291–304, doi:10.1016/j.pepi.2003.06.007.

Seto, Y., D. Hamane, T. Nagai, and K. Fujino (2008), Fate of carbonates within oceanic plates subducted to the lower mantle, and a possible mechanism of diamond formation, *Phys. Chem. Miner.*, *35*(4), 223–229, doi:10.1007/s00269-008-0215-9.

Shcheka, S. S., M. Wiedenbeck, D. J. Frost, and H. Keppler (2006), Carbon solubility in mantle minerals, *Earth Planet. Sci. Lett.*, *245*(3–4), 730–742, doi:10.1016/j.epsl.2006.03.036.

Skorodumova, N. V., A. B. Belonoshko, L. Huang, R. Ahuja, and B. Johansson (2005), Stability of the $MgCO_3$ structures under lower mantle conditions, *Am. Mineral.*, *90*(5–6), 1008–1011, doi:10.2138/am.2005.1685.

Sleep, N. H., and K. Zahnle (2001), Carbon dioxide cycling and implications for climate on ancient Earth, *J. Geophys. Res.*, *106*(E1), 1373–1399, doi:10.1029/2000JE001247.

Stachel, T., J. W. Harris, G. P. Brey, and W. Joswig (2000), Kankan diamonds (Guinea) II: Lower mantle inclusion parageneses, *Contrib. Mineral. Petrol.*, *140*(1), 16–27, doi:10.1007/s004100000174.

Stagno, V., and D. J. Frost (2010), Carbon speciation in the asthenosphere: Experimental measurements of the redox conditions at which carbonate-bearing melts coexist with graphite or diamond in peridotite assemblages, *Earth Planet. Sci. Lett.*, *300*(1–2), 72–84, doi:10.1016/j.epsl.2010.09.038.

Syracuse, E. M., P. E. van Keken, and G. A. Abers (2010), The global range of subduction zone thermal models, *Phys. Earth Planet. Inter.*, *183*(1–2 SI), 73–90, doi:10.1016/j.pepi.2010.02.004.

Wood, B. J., A. Pawley, and D. R. Frost (1996), Water and carbon in the Earth's mantle, *Philos. Trans. R. Soc. London A*, *354*(1711), 1495–1511, doi:10.1098/rsta.1996.0060.

Yagi, T., T. Suzuki, and S. Akimoto (1985), Static compression of wüstite ($Fe_{0.98}O$) to 120 GPa, *J. Geophys. Res.*, *90*(B10), 8784–8788, doi:10.1029/JB090iB10p08784.

Yaxley, G. M., and G. P. Brey (2004), Phase relations of carbonate-bearing eclogite assemblages from 2.5 to 5.5 GPa: Implications for petrogenesis of carbonatites, *Contrib. Mineral. Petrol.*, *146*(5), 606–619, doi:10.1007/s00410-003-0517-3.

Yaxley, G. M., and D. H. Green (1994), Experimental demonstration of refractory carbonate-bearing eclogite and siliceous melt in the subduction regime, *Earth Planet. Sci. Lett.*, *128*(3–4), 313–325, doi:10.1016/0012-821X(94)90153-8.

Zhou, D., R. A. Metzler, T. Tyliszczak, J. H. Guo, M. Abrecht, S. N. Coppersmith, and P. Gilbert (2008), Assignment of polarization-dependent peaks in carbon K-edge spectra from biogenic and geologic aragonite, *J. Phys. Chem. B*, *112*(41), 13,128–13,135, doi:10.1021/jp803176z.

D. Antonangeli, A. L. Auzende, K. Benzerara, E. Boulard, H. Bureau, G. Fiquet, F. Guyot, N. Menguy, G. Morard, and J. Siebert, Institut de Minéralogie et de Physique des Milieux Condensés, Institut de Physique du Globe de Paris, Université Pierre et Marie Curie, UMR 7590, CNRS, Université Paris Diderot, 4 place Jussieu, F-75005 Paris, France. (boulard@stanford.edu)

A. Corgne, Institut de Recherche en Astrophysique et Planétologie, UMR 5277 Université de Toulouse, CNRS, 14 ave. Edouard Belin, F-31400 Toulouse, France.

J. P. Perrillat, Laboratoire de Géologie de Lyon, UMR 5276, Université Claude Bernard Lyon 1, CNRS, ENS Lyon, 2 Rue Raphaël Dubois, F-69622 Villeurbanne, France.